Atmos. Chem. Phys. Discuss., 13, 24171–24222, 2013
www.atmos-chem-phys-discuss.net/13/24171/2013/
doi:10.5194/acpd-13-24171-2013

Atmospheric Chemistry and Physics
Discussions
Open Access

Numerical analysis of the chemical kinetic mechanisms of ozone depletion and halogen release in the polar troposphere

L. Cao[1], **H. Sihler**[2,3], **U. Platt**[2], **and E. Gutheil**[1]

[1]Interdisciplinary Center for Scientific Computing, University of Heidelberg, Heidelberg, Germany
[2]Institute for Environmental Physics, University of Heidelberg, Heidelberg, Germany
[3]Max Planck Institute for Chemistry, Mainz, Germany

Received: 9 July 2013 – Accepted: 2 September 2013 – Published: 13 September 2013

Correspondence to: L. Cao (le.cao@iwr.uni-heidelberg.de)

Published by Copernicus Publications on behalf of the European Geosciences Union.

Abstract

In recent years, the role of halogen species (e.g. Br, Cl) in the troposphere of polar regions is investigated after the discovery of their importance for boundary layer ozone destruction in the polar spring. Halogen species take part in an auto-catalytic chemical cycle including key self reactions. In this study, several chemical reaction schemes are investigated, and the importance of specific reactions and their rate constants is identified by a sensitivity analysis. A category of heterogeneous reactions related to HOBr activate halogen ions from sea salt aerosols, fresh sea ice or snow pack, driving the "bromine explosion". In the Arctic, a small amount of NO_x may exist, which comes from nitrate contained in the snow, and this NO_x may have a strong impact on ozone depletion. The heterogeneous reaction rates are parameterized by considering the aerodynamic resistance, a reactive surface ratio, β, i.e. ratio of reactive surface area to total ground surface area, and the boundary layer height, L_{mix}. It is found that for $\beta = 1$, the ozone depletion process starts after five days and lasts for 40 h for $L_{mix} = 200$ m. Ozone depletion duration becomes independent of the height of the boundary layer for about $\beta \geq 20$, and it approaches a value of two days for $\beta = 100$.

The role of nitrogen and chlorine containing species on the ozone depletion rate is studied. The calculation of the time integrated bromine and chlorine atom concentrations suggests a value in the order of 10^3 for the [Br]/[Cl] ratio, which reveals that atomic chlorine radicals have minor direct influence on the ozone depletion. The NO_x concentrations are influenced by different chemical cycles over different time periods. During ozone depletion, the reaction cycle involving the $BrONO_2$ hydrolysis is dominant. A critical value of 0.002 of the uptake coefficient of the $BrONO_2$ hydrolysis reaction at the aerosol and saline surfaces is identified, beyond which the existence of NO_x species accelerate the ozone depletion event – for lower values, deceleration occurs.

1 Introduction, state of the art, and objectives

Since the 1980s, it has been reported that in polar regions, the amount of ozone in the tropospheric layer may reduce from the normal value of tens of ppb (ppb = parts per billion) to less than 1 ppb or even under the detection limit during the polar spring season (Oltmans, 1981; Barrie et al., 1988, 1989; Oltmans et al., 1989; Helmig et al., 2007, 2012). The observed depletion time varies from several hours to days. During the ozone depletion event, a sudden release of halogen species (X, X_2, XY, XO, HOX, where X and Y denote halogen atoms such as Br and Cl) has been detected in both the Arctic and Antarctic (Hausmann and Platt, 1994; Kreher et al., 1997; Tuckermann et al., 1997; Hönninger and Platt, 2002; Frieß et al., 2004; Wagner et al., 2007).

Halogen species are involved in an auto-catalytic chemical cycle, leading to ozone depletion (Wayne et al., 1995; Platt and Janssen, 1995; Platt and Moortgat, 1999; Platt and Hönninger, 2003). The activation of halogens from the aerosols or the ice surface by HOBr leads to a sudden increase of bromine concentration, which is called "bromine explosion" (Platt and Janssen, 1995; Platt and Lehrer, 1997; Wennberg, 1999). A detailed review of the chemical reaction mechanism about the lower tropospheric ozone depletion has been described fully by Platt and Hönninger (2003), Simpson et al. (2007), and Abbatt et al. (2012).

A number of numerical studies have been conducted since the 90's of the last century. Box models were used to capture the temporal evolution of the chemical species (Fan and Jacob, 1992; Sander and Crutzen, 1996; Tang and McConnell, 1996; Sander et al., 1997; Michalowski et al., 2000). More recently, box model studies (Sander et al., 2006; Morin et al., 2008) focus on the role of calcium carbonate precipitation in the triggering of bromine explosion. The coupling of HO_x, NO_x and halogen chemistry is also investigated (Chen et al., 2007; Bloss et al., 2010; Liao et al., 2011). In these box models, different techniques have been applied explicitly or implicitly to include the key heterogeneous reactions occurring at the aerosol surface or at the snow/ice surface.

Most of the models mentioned above apply the deposition and emission of the halogen species to represent the recycling of halogens at the ice/snow surface (Sander and Crutzen, 1996; Chen et al., 2007; Bloss et al., 2010). Recently, a quasi-liquid layer on snow/ice is studied (Boxe and Saiz-Lopez, 2008; Thomas et al., 2011; Toyota et al., 2013), accounting for the aqueous reactions in the liquid-like layer and also the gas transfer between the ice/snow surface and the ambient/interstitial gas. However, laboratory research of Huff and Abbatt (2000, 2002) for the activation of Br_2 and BrCl on ice surfaces suggests that the heterogeneous reaction between the gas molecules (HOBr) and the adsorbed compounds (Br^-) at the ice surface closely resembles a mechanism of collision on the solid surface, which is of first order. This implies that the halide-ice reactive surface behaves more like a solid rather than a liquid layer, and the transfer of the gas to the ice surface is the rate-determining step. Therefore, the present study includes a deposition and emission approach.

The coupled snow-gas phase chemistry is intensely studied by Thomas et al. (2011) using a 1-D snow-atmosphere model (MISTRA-SNOW) developed from the 1-D atmospheric boundary layer model MISTRA (Piot and von Glasow, 2008, 2009). In the MISTRA-SNOW model simulation, special attention is paid to the interaction between bromine and nitrogen containing species over the snow covered regions. The importance of the bromine reactivation on aerosol and snow is also addressed. Some researchers tried to consider the transport properties using different simple assumptions to account for turbulence in 3-D simulations (Zeng et al., 2003; Yang et al., 2008, 2010; Zhao et al., 2008; Toyota et al., 2011). The coupling of bromine chemistry and wind speed as well as air mass temperature is parameterized in these 3-D models, confirming the connection between bromine explosion, ozone depletion phenomenon and the local atmospheric conditions.

However, insufficient results are available on the analysis of the chemical reaction mechanism. Little is known about the relative importance of each reaction in the mechanism at different times, and the role of physical properties, such as the influence of boundary layer height, is not clear enough. Moreover, the present literature lacks a detailed discussion on how ozone depletion is altered by the presence of NO_x. The main objectives of the present research are

1. The study of the temporal variation of the chemical species and reaction rates, and thus, identify the dominant reaction cycles at different time during the ozone depletion event.
2. Identification of the significance of each chemical reaction and transport features by sensitivity analysis.
3. Investigation of the role of NO_x and chlorine chemistry on bromine release and ozone depletion.
4. Study of the influence of the height of the boundary layer and surface properties, such as the HOBr uptake coefficient.

2 Mathematical model and methods

The present model consists of a system of homogeneous chemical reactions, and it may be written in the form

$$\frac{\mathrm{d}\boldsymbol{c}}{\mathrm{d}t} = \boldsymbol{f}(\boldsymbol{c}, \boldsymbol{k}) \qquad (1)$$

with $\boldsymbol{c}|_{t=0} = \boldsymbol{c}_0$, where $\boldsymbol{c}$ denotes the species concentration column vector. Equation (1) may represent complex chemical processes, $\boldsymbol{k}$ is the vector of the reaction rate constants and t denotes time. Solution of the stiff ordinary differential Eq. (1) is achieved using the software KINAL (Turanyi, 1990), which is an open-source software programmed in FORTRAN language solving the system of chemical kinetic equations. A fourth order semi-implicit Runge-Kutta method is used to solve the governing equations.

2.1 Sensitivity analysis

In a complex chemical system, it is difficult to see, which chemical reactions are more important than others. However, if this information is available, it would help to gain insight and better understanding of the kinetic behavior. In this situation a sensitivity analysis is helpful to gain deeper knowledge about the chemical reactions system. One element of the local relative sensitivity matrix can be written as

$$S_{ij} = \frac{\partial \ln c_i}{\partial \ln k_j}, \tag{2}$$

where c_i is the concentration of the i-th species, and k_j is the rate constant of j-th reaction. The concentration sensitivity, S_{ij}, is a function of time, and it represents the effect of the i-th concentration change caused by the j-th reaction rate change at different times. The matrix decomposed method (Valko and Vajda, 1984) is embedded in KINAL to perform the sensitivity analysis.

2.2 Reaction schemes

The reactions are listed in the Supplement and the reaction rates are calculated at $T = 258\,\mathrm{K}$ at atmospheric pressure. Reactions numbers in the following text refer to the table in the Supplement. Three different detailed chemical reaction schemes are studied. The first one concerns bromine containing species only. The second reaction scheme is an extension of the first one, where nitrogen containing species are added, and the third chemical reaction scheme also includes chlorine reactions. Details about the chemical mechanisms and the initial conditions are given in the result section.

The total halogen stock is determined by the heterogeneous reactions

$$\mathrm{HOBr} + \mathrm{HX} \xrightarrow{\text{aerosol}} \mathrm{BrX} + \mathrm{H_2O} \qquad \text{(R14, R128)}$$

$$\mathrm{HOBr} + \mathrm{H^+} + \mathrm{X^-} \xrightarrow{\text{ice/snow}} \mathrm{BrX} + \mathrm{H_2O}, \qquad \text{(R15, R129)}$$

where (R14) and (R15) refer to X=Br and (R128) and (R129) to Cl. Thus, it is essential to precisely parameterize the multiphase reaction rates.

2.2.1 Heterogeneous reaction for aerosols

By absorbing gaseous HOBr and HX, the liquid aerosols containing high concentrations of sea salt could offer a possible location for (R14) and (R128) to occur (Sander and Crutzen, 1996). Active halogen species BrX are reformed at the aerosol surface, and then, they are emitted into the surrounding environment.

According to Schwartz (1986), the production rate of Br_2 molecules for (R14) is given as

$$\frac{\mathrm{d}[\mathrm{Br_2}]}{\mathrm{d}t} = -\frac{\mathrm{d}[\mathrm{HOBr}]}{\mathrm{d}t} = k_{\mathrm{R14}}[\mathrm{HOBr}] \tag{3}$$

with the first order heterogeneous reaction rate constant

$$k_{\mathrm{R14}} = \left(\frac{a}{D_g} + \frac{4}{v_{\mathrm{therm}}\gamma}\right)^{-1}\alpha_{\mathrm{eff}}. \tag{4}$$

The term a/D_g in Eq. (4) represents the molecular diffusion limit, where D_g is the molecular diffusivity in the gas phase. In the present model, $D_g = 0.2\,\mathrm{cm^2\,s^{-1}}$, and $a = 0.45\,\mu\mathrm{m}$ is the typical aerosol radius. The remaining contribution on the RHS of Eq. (4) accounts for the collision frequency at the surface. The molecular mean speed v_{therm} of HOBr is given by $v_{\mathrm{therm}} = \sqrt{\frac{8RT}{\pi M_{\mathrm{HOBr}}}}$, where M_{HOBr} is the molar mass of HOBr. R is the universal gas constant and T is the absolute temperature (258 K in the model). γ in Eq. (4) denotes the uptake coefficient of HOBr on sea salt aerosols. Considering Eq. (4), it is seen that for aerosols with low γ, thermal collision induced reactions are favored, while in case of a high value of γ, there will be limitations due to diffusion.

Title Page
Abstract Introduction
Conclusions References
Tables Figures
◀| |▶
◀ ▶
Back Close
Full Screen / Esc
Printer-friendly Version
Interactive Discussion

The surface-volume coefficient, α_{eff}, is the ratio of the total aerosol surface area, A_{aerosol}, and the total volume, V

$$\alpha_{\mathrm{eff}} = \frac{A_{\mathrm{aerosol}}}{V}. \tag{5}$$

The value of the uptake coefficient, γ, and the surface-volume coefficient, α_{eff}, for heterogeneous reaction rate of (R14) must be evaluated.

For Reaction (R14), the production of Br_2 is limited by the absorption of both gaseous HOBr and HBr in the suspended aerosol particles. The HOBr uptake coefficient γ to the bulk of liquid phase can be expressed in the form of Eq. (6) according to Hanson et al. (1994)

$$\frac{1}{\gamma} = \frac{1}{\alpha} + \frac{v_{\mathrm{therm}}}{4\mathrm{H}^{*}RT\sqrt{k^{\mathrm{I}}_{\mathrm{liq}}D_{\mathrm{liq}}}\,f(q)}. \tag{6}$$

Here, α is the accommodation coefficient taken to be unity in the present study. The effective Henry constant, H^{*}, is applied for the species, which can dissociate in the liquid solutions, and it has the value of $1.7\times10^{4}\ \mathrm{mol\,(L\,atm)^{-1}}$ for HOBr. $k^{\mathrm{I}}_{\mathrm{liq}}$ is the first order liquid reaction rate constant of HOBr / HBr reaction, and it can be calculated as $k^{\mathrm{I}}_{\mathrm{liq}} = k^{\mathrm{II}}_{\mathrm{liq}}\,[\mathrm{HBr}]_{\mathrm{liq}} = k^{\mathrm{II}}_{\mathrm{liq}}\,\mathrm{H}^{*}_{\mathrm{HBr}}\,P_{\mathrm{HBr}}$. $k^{\mathrm{II}}_{\mathrm{liq}}$ is the second order liquid reaction rate constant, and its value is $5\times10^{4}\ \mathrm{L\,(mol\,s)^{-1}}$. The effective Henry constant of HBr for HOBr / HBr reaction has the value of $3\times10^{8}\ \mathrm{mol\,(L\,atm)^{-1}}$ in the model. P_{HBr} is the partial pressure of gaseous HBr. For 10 ppt HBr, $P_{\mathrm{HBr}} = 10^{-11}$ atm. D_{liq} in Eq. (6) denotes the liquid HOBr diffusion coefficient, which is taken to be $5\times10^{-6}\ \mathrm{cm^{2}\,s^{-1}}$. The function $f(q) = \coth(q) - (1/q)$, where $q = a\sqrt{k^{\mathrm{I}}_{\mathrm{liq}}/D_{\mathrm{liq}}}$, and a is the typical aerosol radius. Thus, $\gamma = 0.12$ is obtained for a gas mixing ratio of 10 ppt HBr. If the aerosol particles are assumed to be uniformly distributed, using the data provided by Staebler et al. (1999), the aerosol volume concentration is calculated to be $10^{-11}\ \mathrm{cm^{3}\,cm^{-3}}$, and $10^{-6}\ \mathrm{cm^{2}}$ effective aerosol surface area is offered in each $\mathrm{cm^{3}}$ volume of air, which corresponds to

$\alpha_{\text{eff}} = 10^{-6}\,\text{cm}^{-1}$. The first-order reaction rate constant for Reaction (R14) can then be calculated as $k_{\text{R14}} = 6.14 \times 10^{-4}\,\text{s}^{-1}$ for 10 ppt HBr mixing ratio.

Considering the chlorine containing mechanism in (R128), BrCl is produced via the corresponding heterogeneous reaction. Similarly, if the HCl mixing ratio is 10 ppt, the first-order reaction rate $k_{\text{R128}} = 1.61 \times 10^{-5}\,\text{s}^{-1}$ is obtained with $k^{\text{II}}_{\text{liq}} = 10^5\ \text{L}\,(\text{mol}\,\text{s})^{-1}$ and $H^* = 3 \times 10^6\,\text{mol}\,(\text{L}\,\text{atm})^{-1}$ for HOBr / HCl reaction.

2.2.2 Heterogeneous reaction for ice/snow packs

For Reactions (R15) and (R128), in which the ice/snow pack offers the possible reaction site, the change in concentration of HOBr depends on the deposition velocity, v_d, at the ice/snow surfaces, the typical height of the mixing layer, L_{mix}, and the total reactive surface area offered by ice/snow, which is denoted by a reactive surface ratio coefficient, β

$$\frac{\text{d[HOBr]}}{\text{d}t} = -k_\text{d}[\text{HOBr}], \qquad (7)$$

where the deposition rate constant k_d

$$k_\text{d} = \frac{v_\text{d}}{L_{\text{mix}}}\beta. \qquad (8)$$

The deposition velocity v_d is governed by the sum of three resistances (Seinfeld and Pandis, 1998): the aerodynamic resistance r_a, the quasi-laminar layer resistance r_b and the surface resistance r_c:

$$v_\text{d} = (r_a + r_b + r_c)^{-1}. \qquad (9)$$

r_a shows the resistance of turbulent transport of bringing the gas from the atmosphere down to the surface, and it is given as $1/(u\kappa^2)(\ln(z/z_0))^2$, where u is the wind speed for which the value 8 m s^{-1} is used (Beare et al., 2006), $\kappa = 0.4$ is the von Karman's constant. z is the height of the surface layer, which is 10 % of the boundary layer height. z_0 is the surface roughness length, and 10^{-5} m is used for the ice surface (Stull, 1988; Huff and Abbatt, 2000, 2002). Thus, the value of r_a depends on the local transport properties (wind speed, boundary layer, ...). The quasi-laminar layer resistance, r_b, represents the ability of molecular diffusion to tranfer gas across a liquid-laminar layer above the surface, and it is given as $r_b = z_0/D_g$. r_c is the resistance due to the reaction loss, and it expressed as $4/(v_{\text{therm}}\gamma)$. A constant uptake coefficient of $\gamma = 0.06$ is taken after Sander and Crutzen (1996); this includes the assumption that H^+ and halogen ions are inexhaustible at the ice/snow surface.

L_{mix} in Eq. (8) stands for the typical height of the stable boundary layer. Typical magnitudes of the stable boundary layer height observed in polar regions range from a near zero value to over 1000 m (Stull, 1988), depending, for instance, on the wind speed and the temperature inversion intensity. In the present model, different boundary layer heights of 200 m (suggested in Beare et al. (2006) and used in Evans et al., 2003), 500 m (used in Oltmans et al., 2012) and 1000 m (used in Lehrer et al., 2004) are considerd. The deposition velocity for the three boundary layer heights is 0.605 cm s^{-1}, 0.536 cm s^{-1} and 0.491 cm s^{-1}, respectively. These values are in the reasonable range of the HOBr deposition velocity (Sander and Crutzen, 1996; Adams et al., 2002; Yang et al., 2005).

A reactive surface ratio coefficient β is introduced in Eq. (8), representing the ratio of total reactive surface area offered by the ice/snow surface and the flat surface area. For a flat surface of pure ice, β equals unity. However, considering the porous properties of the contaminated snow above the ice surface, larger surface area may be offered by the ice/snow surface. Besides, the surface physical structure and the roughness may also increase the reactive surface area, for instance, through frost flowers because of their sharp angular features (Rankin et al., 2002). The lifted snow pumped by the wind near the surface may also increase the total reactive surface area. Because of the uncertainty of the reactive surface area offered by the saline surface, a parameter study is conducted with the consideration of a proper range of β.

If the chlorine mechanism is discarded, all HOBr molecules residing at the ice/snow surface are converted into Br_2 through Reaction (R15), and the Br_2 is emitted into the ambient air. For $\beta = 1.0$, the reaction rate constant k_{R15} for Reaction (R15) is calculated as $3.03 \times 10^{-5}\,s^{-1}$, $1.072 \times 10^{-5}\,s^{-1}$ and $4.91 \times 10^{-6}\,s^{-1}$ for the boundary layer heights $L_{mix} = 200$ m, 500 m and 1000 m, respectively.

However, if the chlorine mechanism is added, reaction

$$HOBr + H^+ + Cl^- \xrightarrow{snow/ice} BrCl + H_2O \qquad (R129)$$

competes with Reaction (R15) for the HOBr molecules, and the reaction rate ratio, $K_{Br_2/BrCl} = k_{R15}/k_{R129}$ of Reactions (R15) and (R129) determines the formation ratio of Br_2 and BrCl molecules through the heterogeneous activation from the ice/snow pack. The value of $K_{Br_2/BrCl}$ varies between 0.8 to 1.4 (Foster et al., 2001). Michalowski et al. (2000) found that the ozone depletion rate is very sensitive to the production rate ratio of Br_2 and BrCl. Therefore, the relation between the production rate ratio and ozone depletion time is investigated in the present study, whereas the default value is taken to be unity.

In the next section, results of the numerical computations are presented with emphasis on the different reaction schemes discussed above, and their influence on ozone depletion is evaluated.

3 Results

First, the mechanism without any NO_x and chlorine related reactions is analyzed. The chemical reaction scheme involves 55 chemical reactions (Reactions (R1) through (R55) in the Supplement) and 30 species, called “bromine only mechanism”. Then, 31 reactions (Reactions R56 through R86) and 9 nitrogen containing species are added in order to investigate the effect of NO_x species. Similar constant values of uptake coefficient ($\gamma = 0.06$) are taken for these NO_x related heterogeneous Reactions (R83), (R85) and (R86). Since NO_x is converted to PAN (peroxyacytyl nitrate), which can be hardly photolyzed, fluxes of nitrogen containing species produced from the snow are added to the model (see Table 1). The emission rates of NO, NO_2, H_2O_2 and HCHO are estimated based on the measurements (Jones et al., 2000, 2001; Jacobi et al., 2002), and the production ratio of HONO and NO_2 is 1.0 (Grannas et al., 2007). The photolysis of nitrate in the snow pack is suggested as the major source of the nitrogen containing fluxes. Finally, 49 chlorine related reactions (Reactions R87 through R135) and 10 chlorine containing species are included. When the latter mechanism is used, the time integral concentrations of active bromine and chlorine radicals during the ozone depletion are determined. The average photolysis reaction rates are computed using Röth's model (Röth, 1992, 2002) under the condition that the Solar Zenith Angle (SZA) equals 80 degrees.

The initial gas phase species mixing ratios are listed in Table 2 (ppm = parts per million, ppt = parts per trillion). The prescribed initial trigger of bromine species in air is 0.3 ppt Br_2 and 0.01 ppt HBr. This small amount of active bromine could come from the degradation of natural organohalogen compounds (e.g. CH_3Br). All other species not listed have initial concentration of zero (except for natural air).

3.1 Bromine only mechanism

Figure 1 displays the modeled concentrations of the relevant species as a function of time for three different boundary layer heights of 200, 500, and 1000 m, and Fig. 2 shows a column presentation of Fig. 1a. It can be seen that ozone depletion starts after five days and lasts for about 40 h for a 200 m boundary layer thickness. Before day five, little ozone is consumed. At this early stage, HOBr and BrO concentrations show exponential growth, and these two species constitute the majority contributions of bromine species. Due to the existence of ozone, the active Br atoms are instantly converted to BrO, and thus, they can hardly be observed at this time. As the concentration of HOBr is increasing, a large amount of reactive bromine is triggered from the saline surface and sea salt aerosols, leading to an explosive increase of the total bromine concentration and a rapid decrease of ozone. After six days, BrO builds up to reach a peak level of 60 ppt, and then it rapidly decreases. When the HOBr concentration increases to its maximum value of about 70 ppt, the ozone mole fraction falls down below 1 ppb. As HOBr falls rapidly, the Br atom concentration abruptly builds up to be the main constituent of the bromine stock, which increases to its maximum value of about 170 ppt. This large amount of Br then is removed by the aldehydes (for instance HCHO and CH_3CHO) in the natural air, forming HBr. At the end of the depletion event, a high level of HBr is left in the air, which is confirmed by the aerosol measurements of Langendörfer et al. (1999).

When the boundary layer grows to the height of 500 m and 1000 m as in situation (b) and (c), respectively, cf. Fig. 1, the strongest ozone depletion occurs after 15 days or even more than 30 days with the same initial conditions and the depletion itself is extended to about 3–5 days. The principal profiles of bromine species concentrations are similar to those in situation (a), but the peak values are considerably lower. The maximum values of BrO are in the range of 30–40 ppt. The result for 1000 m boundary layer height may be compared with a numerical study of Lehrer et al. (2004), who find the depletion to end after 40 days. This value agrees well with a previous study (Cao and Gutheil, 2011) neglecting the aerodynamic resistance in both of these studies. Since the typical height of stable boundary layers measured in polar regions vary from 100 m to 500 m (Stull, 1988), the remainder of the study concerns a boundary layer height of 200 m.

Considering the temporal behavior of the species as discussed above, the whole ozone depletion process may be divided into three time periods. At the beginning of the event, the gaseous halogen concentrations in the air are low, only a small fraction of ozone is consumed, this period may be called “induction stage”. It is followed by the “depletion stage”, where a large amount of inert halogens are triggered from sea salts by the frequent collisions between the saline surface and HOBr molecules. The ozone in the lower troposphere is severely consumed at this stage and the depletion rate is in the order of 1 ppb h^{-1}. In the last time period, the “end stage”, ozone is almost completely depleted. The remaining halogen species are hydrogen halides, and the total halogen concentration keeps stable. Different values of the initial bromine trigger concentration have been tested. For a reduced value of initial bromine concentration of 0.1 ppt, the “induction stage” is prolonged, and for a higher initial value of 0.5 ppt, it is reduced, whereas the time for the depletion itself is hardly affected. This means that the ozone depletion is caused by the activated bromine from the sea salts, whereas the initial bromine concentration serves as a trigger to the ozone depletion event.

The reactions directly affecting ozone concentration are listed in Table 3, note that the complete mechanism is provided in the Supplement. Reactions (R3), (R7), (R30), and (R54) cause ozone formation, whereas Reactions (R1), (R5), (R27), (R31), and (R36) lead to ozone depletion. The temporal evolution of these ozone relevant reaction rates are plotted in Fig. 3 for the case of 200 m boundary layer height in logarithmic scale. The relevance of these reactions is discussed below in connection with the sensitivity analysis, which reveals that the reactions discussed here have a high relative sensitivity and therefore, they dominate the entire process under consideration. In the top part of the figure, ozone forming reactions are displayed, and in the bottom part, the rates for ozone depletion reactions are depicted in reverse vertical axial direction. It can be seen that during the ozone depletion period from day 5 to day 7, the fastest enhancement reaction is (R7) while the strongest depletion is caused by (R5). These two reactions combine to form the most effective ozone cycle. Due to the reactive Br atoms formed by the self-reactions (R8) and (R9), the peak value of the (R5) reaction rate is higher than that of (R7). Therefore, ozone tends to decrease in this fastest cycle. The second most efficient ozone cycle consists of formation Reaction (R3) and depletion Reaction (R1). This cycle is more dominant before day 3. When the ozone depletion event starts, and after day 7, this cycle is at least two orders of magnitude less effective than the fastest cycle.

In the present study, the relevance of different chemical reaction steps is discussed in the framework of a sensitivity analysis (see Eq. 2), which will be used in a future investigation to reduce the present mechanism to a skeletal reaction scheme for application in future 3-D simulations. Figure 4 shows the relative sensitivities for ozone and BrO concentrations at day 6, which is the time, when major ozone depletion occurs. Red and blue bars show the sensitivity coefficients for BrO and for O_3, respectively, where it can be seen that they have opposite signs, which means that ozone is destroyed/formed as BrO is built up/consumed, a negative sign corresponds to depletion. Reactions (R5) and (R7), which constitute the fastest ozone cycle as mentioned above, have a high impact on the ozone and BrO concentrations. HOBr production and destruction reactions, (R10) and (R11), are important since HOBr is involved in the heterogeneous bromine liberation process. The heterogeneous reactions, (R14) and (R15), are also crucial for the same reason. This means that it is very important to have a good knowledge of the chemical reaction rates of these reaction steps because of their dominance of the ozone depletion mechanism.

The temporal sensitivity evolution of ozone concentration for boundary layer height L_{mix}, saline surface uptake coefficient γ and reactive surface ratio β is displayed in Fig. 5. When the depletion process starts after 5 days, the absolute values of these sensitivities increase sharply and reach their peaks at around day 7 (cf. Fig. 5). The sensitivity of γ is smaller compared to the other two parameters because at the ice/snow surface, collision kinetics is less dominant compared to the transport of the air. Since all the physical properties considered here affect the ozone depletion through the heterogenous reactions, it is demonstrated that the heterogeneous liberation process is very important throughout the ozone depletion state. Therefore, the effect of these parameters are studied in more detail.

The relative sensitivity of L_{mix} is positive, which means that for increased boundary layer height, the ozone depletion occurs later and less abrupt. This is consistent with the results shown in Fig. 1. Similarly, the negative sensitivities of γ and β cause a decrease of the ozone concentration with increased γ and β, which means that the ozone depletion is enhanced for higher values. This can be explained as follows: if the reaction probability between HOBr and the reactive surface is larger (i.e. a more reactive surface area is offered for the heterogeneous reactions), more bromine atoms are released, leading to the acceleration of the ozone depletion.

The reactive surface area ratio, β, is influenced by the physical structure and the roughness of the fresh ice surface covered by snow, which affects the heterogeneous Reaction (R15). Figure 6 shows the variation of the ozone depletion time with the reactive surface ratio β. The vertical axis represents the total time needed until ozone mixing ratio is less than 4 ppb (10 % of the initial mixing ratio), and the horizontal axis shows the value of β in log scale. Obviously, in different boundary layer conditions, when $\beta < 10$, the increase of β significantly reduces the total time including induction and depletion. All the depletion events with different boundary layer heights are completed within ten days if $\beta > 5$. When β approaches 100, all curves approximate the minimum limit of two days. This means that the maximum ozone depletion event rate caused by local chemistry is two days at 200 m boundary layer height. From some observations (Bottenheim et al., 1986; Tuckermann et al., 1997; Jones et al., 2006), extremely rapid ozone decrease with a drop of 30 ppb within several hours is found. However, it is usually assumed that most of this rapid decrease is caused by the transport of ozone-lacking air parcels to the measuring location (Simpson et al., 2007). To solve this question of chemistry versus transport, the consideration of the horizontal transport process is needed, which is beyond the scope of the present study.

The following sections concern the extension of the present bromine mechanism through chemical reactions, which include NO_x and chlorine.

3.2 NO_x Related chemical reaction mechanism

The role of NO_x chemistry may be investigated by adding Reactions (R56) to (R86) to the present chemical reaction system (see Supplement). The NO_x mechanism adds 9 chemical species and 31 chemical reactions to the bromine mechanism. In Fig. 7, ozone, bromine and NO_x concentration profiles are plotted for $L_{mix} = 200$ m. During the ozone destruction period between days 3 and 4.5, the initial 15 ppt NO_x and fluxes of nitrogen containing species from the snow (see Table 1) are converted into $BrONO_2$ and other nitrogen containing species such as $BrNO_2$. The major sink of the nitrogen is PAN. Moreover, because an additional HOBr flux is generated by the $BrONO_2$ hydrolysis process (R83) and (R86) at the aerosol surfaces and the ice/snow pack, the peak value of HOBr activated from sea salts reaches more than 110 ppt compared to 70 ppt released by the chemical reaction mechanism without NO_x reactions, see Fig. 7b. It is illustrated that the total bromine concentration increases from about 180 ppt to approximately 300 ppt. This large value approaches the extreme bromine observation value of about 260 ppt reported by Impey et al. (1999). Figure 7 shows that the ozone depletion process starts after 3 days and ends before day 4.5. Thus, the induction period is shorter by about 2 days whereas the depletion stage is about the same compared with the results using the bromine only mechanism.

The reactions strongly and directly affecting NO_x concentrations are listed in Table 4, and their reaction rate evolutions are shown in Fig. 8. It is seen that NO_x concentrations are largely influenced by different reaction cycles at different time stages. Table 5 gives a summary of the chemical reaction cycles affecting NO_x concentrations. In the early induction stage before day 3, formation Reaction (R63) and depletion Reaction (R62) constitute the most effective NO_x cycle (N-I). When ozone depletion starts, due to a strong increase of the bromine concentration, the Reactions (R79), (R81) and (R85) related to $BrONO_2$ become more important. Considering the hydrolysis Reactions (R83) and (R86) of $BrONO_2$, the most efficient NO_x cycle (N-II) during ozone depletion constitutes. Since most of the NO_x molecules are involved in cycle (N-II) at this time, the reaction rates of cycle (N-I) shortly drop. As depletion ends after day 4.5 with the sharp decrease of the reaction rates in cycle (N-II), the NO_x cycle (N-III) consisting of (R77) and (R82) is prominent. In cycle (N-III), $BrNO_2$ is the major product, which is also observed in Fig. 7a.

The relative sensitivities of NO_x concentrations at day 4, which is within the ozone depletion stage (between day 3 and 4.5) is displayed in Fig. 9. PAN is the major sink of nitrogen. Reaction (R75), which modifies the CH_3CO_3 concentration, decreases the PAN mixing ratio. Reaction (R76) leads to formation of PAN, and therefore, the NO_x concentration is reduced. Reactions (R56) and (R68), which determine the gaseous NO and NO_2 ratio, are also crucial. It is worth noting that the hydrolysis reaction of $BrONO_2$ at the aerosol surface (R83) has a large impact on NO_x concentrations at this time. Considering (R83) with moderate $BrONO_2$ formation (R79) and consumption Reactions (R81), the importance of cycle (N-II) during the ozone depletion period is demonstrated.

The relative sensitivities of the O_3 concentration for reactions related to NO_x at day 4 are shown in Fig. 10. The importance of each reaction on O_3 concentration is similar to those for the NO_x concentrations shown in Fig. 9. However, the sensitivities for PAN related reactions (Reactions R75 and R76) are lower for ozone compared to NO_x. This is because for the ozone concentration, the consumption and formation of PAN are not as important as they are for NO_x concentrations as discussed above. For ozone, the most important NO_x related reaction is the hydrolysis reaction of $BrONO_2$ at the aerosol surface (R83), since in this reaction, the HOBr concentration is enhanced, leading to a reduced ozone concentration.

The importance of nitrogen related reactions versus bromine related reactions at day 4 is shown in Figs. 10 and 11. The bromine related reactions have a much higher sensitivity for ozone depletion compared to nitrogen related reactions at this time. A comparison of the sensitivity of bromine related reactions at day 6 for the bromine only mechanism, cf. Fig. 4, and the present mechanism at day 4 shows a relative higher sensitivity of the heterogeneous Reaction (R15) due to the increased HOBr concentration in the NO_x mechanism (see Fig. 7); this leads to a reduced importance of Reactions (R5) and (R7) in the mechanism including NO_x related reactions. However, note that the time until O_3 depletion starts is considerably influenced by the presence of NO_x as shown in Fig. 12, which is discussed below.

Nitrogen containing species are involved in both the ozone production and the destruction cycle. NO_x species may help to accelerate the ozone depletion by the processes related to halogen nitrates ($XONO_2$). The formation of halogen nitrates and the following hydrolysis decomposition are suggested by Sander et al. (1999)

$$XO + NO_2 \rightarrow XONO_2 \tag{R79}$$

5 $$XONO_2 + H_2O \xrightarrow{mp} HOX + HNO_3, \tag{R83, R86}$$

where ”mp” denotes multi-phase reactions, i.e. reactions at the aerosol and at the ice/snow surface.

Halogen nitrates formed in (R79) are rather easily decomposed by hydrolysis at the sea salt aerosol surface through (R83) or at the saline surface through (R86), producing HOX and HNO_3, respectively. The HNO_3 photolysis reaction rates at the aerosol particle surface is 1–2 orders of magnitude faster than that in the gas phase (Finlayson-Pitts, 2009).

As a consequence, in the case of X=Br, the reaction cycle (I) is obtained

$$\begin{array}{ll}
 & BrO + NO_2 \longrightarrow BrONO_2 \\
 & BrONO_2 + H_2O \xrightarrow{mp} HOBr + HNO_3 \\
 & HNO_3 + h\nu \xrightarrow{aerosol} NO_2 + OH \\
\hline
\text{Net:} & BrO + H_2O + h\nu \xrightarrow{mp} HOBr + OH.
\end{array} \tag{I}$$

15 In cycle (I), BrO is sequestrated into $BrONO_2$, leading to the reduction of BrO amount and the enhancement of HOBr formation. Because of the “bromine explosion” mechanism, an additional gaseous bromine flux is released into the air, speeding up the ozone depletion process.

NO_x species could also be involved in an ozone production cycle (II)

$$\begin{array}{lrcl}
 & HO + CO + O_2 & \rightarrow & CO_2 + HO_2 \\
 & HO_2 + NO & \rightarrow & OH + NO_2 \\
 & NO_2 + h\nu + O_2 & \rightarrow & NO + O_3 \\
\hline
\text{Net:} & CO + 2O_2 + h\nu & \rightarrow & O_3 + CO_2.
\end{array} \tag{II}$$

Most of the ozone in the troposphere is formed through cycle (II). The rate-determining step is the conversion step from NO to NO_2. Volatile organic compounds (VOCs) could also replace HO_2 to oxidize NO to obtain NO_2, but this occurs through a more complex chemical reaction system.

Overall, the net effect on ozone depletion through NO_x species results from the balance between cycle (I) and (II). If the additional bromine flux induced by cycle (I) is strong enough, the ozone depleted in cycle (I) is faster than the ozone formed through cycle (II). In this situation, NO_x species accelerate the whole ozone depletion event, and vice versa.

Thus, if the heterogeneous $BrONO_2$ hydrolysis Reactions (R83) and (R86) are negligible ($\gamma = 0.0001$), which means that only a small amount of additional HOBr molecules can be formed by nitrogen related reactions, the presence of nitrogen containing species will slow down ozone depletion as shown in Fig. 12. In contrast, when the value of the uptake coefficient of $\gamma = 0.06$ is used in Reactions (R83) and (R86), ozone, in fact, is depleted earlier than computed with the bromine only mechanism. A critical turning value for the uptake coefficient of Reactions (R83) and (R86) can be identified at $\gamma = 0.002$. In this situation, the ozone produced by the nitrogen cycle equals the amount of ozone destructed by the additional HOBr induced by nitrogen heterogeneous Reactions (R83) and (R86). Then, no effect of NO_x species on ozone concentration is observed, and the ozone depletion predicted equals the one in the bromine only mechanism.

The next section concerns the influence of chlorine related chemical reactions on ozone depletion.

3.3 Chlorine related mechanism

The detailed mechanism including both nitrogen and chlorine related species consists of 135 chemical reactions among 49 species, see Supplement. For the present computations, the reaction rate ratio $K_{Br_2/BrCl}$, of Br_2 and BrCl from the ice/snow surface, see Reactions (R15) and (R129), equals 1.0, which means half of the deposited HOBr molecules are converted to Br_2 while the other half activate BrCl. Figure 13 shows the major chlorine containing species and ozone concentration profiles versus time for a boundary layer height of 200 m. Compared to the NO_x related mechanism, the consumption of ozone in chlorine related mechanism occurs at approximately the same speed of 1 ppb h^{-1}. The total chlorine concentration amounts to 100 ppt at the end of the event, mostly in the form of HCl. The mixing ratio of gaseous ClO is about 0.8 ppt, which is consistent with Perner et al. (1999)'s measurements at Ny-Ålesund, reporting the ClO mixing ratio to be less than 2 ppt.

A parameter study is conducted for influence of the reaction rate ratio $K_{Br_2/BrCl}$ from the ice/snow surface, cf. (R15) and (R129), on the total ozone depletion time (ozone mixing ratio drops to less than 4 ppb). Figure 14 shows the total ozone depletion time to be about 6.5 days for $K_{Br_2/BrCl} = 2.0$. As the value of this ratio decreases, which means that less Br_2 is produced while more BrCl molecules are released from the ground surface, the ozone depletion event is retarded. When the production ratio is less than 0.2, ozone depletion is hardly observed. This reveals that the ozone depletion time is strongly dependent on the reaction rate ratio $K_{Br_2/BrCl}$ for the formation of Br_2 and BrCl from the ice/snow surface. Adams et al. (2002) found in laboratory research that the major reaction product is Br_2 when the ice surface contains sufficient Br^-, whereas BrCl is released as the major product if Br^- is significantly depleted in the ice or snow pack before ozone is consumed. Therefore, it can be concluded that the chemical composition of the ground surface might be important for the ozone depletion rate.

The change of active bromine and chlorine radical concentrations with time versus ozone concentration are plotted in Fig. 15. As the ozone depletes, an exponential increase of the active bromine radicals is observed, whereas the enhancement of Cl is approximately steady. Thus, the destruction of ozone is dominantly dependent on Br atoms and not on the Cl atoms. The calculated ratio of [Br/Cl] during ozone depletion is of the order 10^3. This means that more than 99 % of the ozone is consumed directly by Br radicals. Previous experimental studies using the VOC decay measurement method suggest various values for the [Br] / [Cl] ratio, ranging from tens to more than ten thousand (Jobson et al., 1994; Solberg et al., 1996; Ramacher et al., 1999; Boudries and Bottenheim, 2000). However, most of the studies find values in the order of some hundreds. Michalowski et al. (2000) suggested that the possible reason for the relatively high modeled value of the [Br/Cl] ratio may be an underestimation of the Cl mixing ratio. Spicer et al. (2002) recommend that an additional unknown Cl source should be assumed, which has not yet been considered in any model study until now.

The present investigation of the influence of chlorine chemistry shows that chlorine containing species have minor direct influence on ozone depletion compared to NO_x and bromine.

4 Conclusions and future research

In this study, the ozone depletion and halogen release mechanism in polar spring is analyzed using detailed chemical reaction schemes and a sensitivity analysis. First, a chemical kinetic mechanism including only bromine species is used, which then is extended to include NO_x and, in a second step, chlorine containing species. To our knowledge this is the first study to separate the influence of NO_x and Cl-species on the bromine explosion mechanism and associated ozone depletion events. When the nitrogen and chlorine containing species are not considered, i.e. in the bromine only mechanism, the temporal change of chemical species concentrations suggests that ozone is completely destroyed after 5 days induction time and 40 hours depletion process assuming a boundary layer height of 200 m. When the boundary layer height increases, the whole depletion process is retarded, and the average principal bromine concentrations are reduced. The importance of the bromine containing reactions on the ozone depletion rate is identified using a relative sensitivity analysis of the chemical reaction rates. It is shown that as the bromine stock in the air is heavily enhanced by the "bromine explosion" mechanism, the heterogeneous reactions related to HOBr play an important role. The physical properties such as reactive surface area offered for the heterogeneous reactions, determine the heterogeneous reaction rate, thus greatly affecting the ozone depletion rates. It is found that the shortest ozone depletion period caused by local chemistry ends after two days.

In model runs including NO_x chemistry, the NO_x concentrations are controlled by different chemical cycles at different time periods. During the depletion process, the most dominant NO_x reaction cycle is related to $BrONO_2$ because of the enhanced bromine concentration in the air. The importance of this chemical cycle is identified by both the study of the reaction rate evolutions and relative sensitivities. A critical value of 0.002 of the uptake coefficient of the $BrONO_2$ hydrolysis reaction at the aerosol and saline surfaces is identified, beyond which the existence of NO_x species accelerate the ozone depletion event, whereas for lower values, retardation occurs. In the simulation including the chlorine related mechanism, according to the calculated time integration of Br and Cl radicals, the number of Cl atoms during depletion is less than 0.1 % of the atomic Br radicals. Therefore, the chlorine containing species has minor direct effect on the ozone loss. A parameter study of the reaction rate ratio, $K_{Br_2/BrCl}$, for Br_2 and BrCl formation through Reactions (R15) and (R129) reveals that the chemical composition of the surface has a strong impact on the ozone depletion rate.

The present study will be continued to develop a multi-dimensional model including transport processes. In order to describe the typical polar stable boundary layer precisely, a fine mesh which basically has the grid size in the order of meters is needed near the ground surface. According to Courant-Friedrichs-Lewy condition (Courant et al., 1928), a time step smaller than 0.1 s is required for a typical polar wind speed of about 10 m s^{-1}. This is difficult to fulfill for the relative long simulation time needed for the ozone depletion.

The present study of ozone depletion reveals that the heterogeneous reactions for the halogen activation are important during the depletion period but not during induction time. Therefore, in a 3-D model, the induction period may be treated as a homogeneous system and the heterogeneous reactions may be activated at the beginning of the depletion period, which makes the 3-D computation much more efficient. Since the duration of ozone depletion is about 1–2 days, the computation on a real time scale then is affordable. Currently, a higher dimensional model including the transport of air parcels and turbulent flow is being developed, and some preliminary results are published by Cao and Gutheil (2011).

Supplementary material related to this article is available online at http://www.atmos-chem-phys-discuss.net/13/24171/2013/acpd-13-24171-2013-supplement.pdf.

Acknowledgements. The authors thank the German Science Foundation (DFG) for financial support through grants GU 255/6-1 and PL 193/10-1.

References

Adams, J. W., Holmes, N. S., and Crowley, J. N.: Uptake and reaction of HOBr on frozen and dry NaCl/NaBr surfaces between 253 and 233 K, Atmos. Chem. Phys., 2, 79–91, doi:10.5194/acp-2-79-2002, 2002. 24180, 24191

Abbatt, J. P. D., Thomas, J. L., Abrahamsson, K., Boxe, C., Granfors, A., Jones, A. E., King, M. D., Saiz-Lopez, A., Shepson, P. B., Sodeau, J., Toohey, D. W., Toubin, C., von Glasow, R., Wren, S. N., and Yang, X.: Halogen activation via interactions with environmental ice and snow in the polar lower troposphere and other regions, Atmos. Chem. Phys., 12, 6237–6271, doi:10.5194/acp-12-6237-2012, 2012. 24173

Aranda, A., LeBras, G., Verdet, G., and Poulet, G.: The BrO+CH_3O_2 reaction: Kinetics and the role in the atmospheric budget, Geophys. Res. Lett., 24, 2745–2748, 1997.

Atkinson, R., Baulch, D. L., Cox, R. A., Crowley, J. N., Hampson, R. F., Hynes, R. G., Jenkin, M. E., Kerr, J. A., Rossi, M. J., and Troe, J.: Summary of evaluated kinetic and photochemical data for atmospheric chemistry, Web version, February 2006, http://www.iupac-kinetic.ch.cam.ac.uk, 2006.

Barnes, I., Becker, K. H., and Overath, R. D.: Oxidation of organic sulfur compounds, in: The tropospheric chemistry of ozone in the polar regions, edited by: Niki, H. and Becker, K. H., Springer Verlag, Berlin, 1993.

Barrie, L. A., Bottenheim, J. W., Schnell, R. C., Crutzen, P. J., and Rasmussen, R. A.: Ozone destruction and photochemical reactions at polar sunrise in the lower Arctic atmosphere, Nature, 334, 138–141, 1988. 24173

Barrie, L. A., den Hartog, G., Bottenheim, J. W., and Landsberger, S.: Anthropogenic aerosols and gases in the lower troposphere at Alert, Canada in April 1986, J. Atmos. Chem., 9, 101–127, 1989. 24173

Beare, R. J., MacVean, M. K., Holtslag, A. A., Cuxart, J., Esau, I., Golaz, J. C., Jimenez, M. A., Khairoutdinov, M., Kosovic, B., Lewellen, D., Lund, T. S., Lundquist, J. K., McCabe, A., Moene, A. F., Noh, Y., Raasch, S., and Sullivan, P. P.: An intercomparison of large-eddy simulations of the stable boundary layer, Boundary-Lay. Meteorol., 118, 247–272, 2006. 24180

Bloss, W. J., Camredon, M., Lee, J. D., Heard, D. E., Plane, J. M. C., Saiz-Lopez, A., Bauguitte, S. J.-B., Salmon, R. A., and Jones, A. E.: Coupling of HO_x, NO_x and halogen chemistry in the antarctic boundary layer, Atmos. Chem. Phys., 10, 10187–10209, doi:10.5194/acp-10-10187-2010, 2010. 24173, 24174

Borken, J.: Ozonabbau durch Halogene in der arktischen Grenzschicht: Reaktionskinetische Modellrechnungen zu einem Fruehjahrsphaenomen, Diploma thesis, Universitaet Heidelberg, 1996.

Bottenheim J. W., Gallant A. C., and Brice K. A.: Measurements of NO_y species and O_3 at 82° N latitude, Geophys. Res. Lett., 13, 113–116, 1986. 24186

Boudries, H. and Bottenheim, J. W.: Cl and Br atom concentrations during a surface boundary layer ozone depletion event in the Canadian High Arctic, Geophys. Res. Lett., 27, 517–520, 2000. 24192

Boxe, C. S. and Saiz-Lopez, A.: Multiphase modeling of nitrate photochemistry in the quasi-liquid layer (QLL): implications for NO_x release from the Arctic and coastal Antarctic snowpack, Atmos. Chem. Phys., 8, 4855–4864, doi:10.5194/acp-8-4855-2008, 2008. 24174

Cao, L. and Gutheil, E.: Modeling of auto-catalytic halogen release and ozone depletion in polar regions, J. Phys.: Conf. Ser., 318, 072006, doi:10.1088/1742-6596/318/7/072006, 2011. 24183, 24194

Chen, G., Huey, L., Crawford, J., Olson, J., Hutterli, M., Sjostedt, S., Tanner, D., Dibb, J., Lefer, B., Blake, N., Davis, D., and Stohl, A.: An assessment of the polar HO_x photochemical budget based on 2003 Summit Greenland field observations, Atmos. Environ., 41, 7806–7820, doi:10.1016/j.atmosenv.2007.06.014, 2007. 24173, 24174

Courant, R., Friedrichs, K., and Lewy, H.: Über die Partiellen Differenzengleichungen der Mathematischen Physik, Math. Ann., 100, 32–74, 1928. 24193

DeMore, W. B., Sander, S. P., Goldan, D. M., Hampson, R. F., Kurylo, M. J., Howard, C. J., Ravishankara, A. R., Kolb, C. E., and Molina, M. J.: Chemical kinetics and photochemical data for use in stratospheric modeling No. 12, Jet Propulsion Laboratory, Pasadena, Publication, 97-4, 1997.

Evans, M., Jacob, D., Atlas, E. L., Cantrell, C. A., Eisele, F., Flocke, F. M., Fried, A., Mauldin, R. L., Ridley, B. A., Wert, B., Talbot, R., Blake, D., Heikes, B., Snow, J., Walega, J. G., Weinheimer, A.J., and Dibb, J.: Coupled evolution of BrO_x-ClO_x-HO_x-NO_x chemistry during bromine-catalyzed ozone depletion events in the arctic boundary layer, J. Geophys. Res., 108, 8368, doi:10.1029/2002JD002732, 2003. 24180

Fan, S. M. and Jacob, D. J.: Surface ozone depletion in Arctic spring sustained by bromine reactions on aerosols, Nature, 359, 522–524, 1992. 24173

Finlayson-Pitts, B. J.: Reactions at surfaces in the atmosphere: integration of experiments and theory as necessary (but not necessarily sufficient) for predicting the physical chemistry of aerosols, Phys. Chem. Chem. Phys., 11, 7760–7779, 2009. 24189

Foster, K. L., Plastridge, R. A., Bottenheim, J. W., Shepson, P. B., Finlayson-Pitts, B. J., and Spicer, C. W.: The role of Br_2 and BrCl in surface ozone destruction at polar sunrise, Science, 291, 471–474, 2001. 24181

Frieß, U., Hollwedel, J., König-Langlo, J., Wagner, T., and Platt, U.: Dynamics and chemistry of tropospheric bromine explosion events in the Antarctic coastal region, J. Geophys. Res., 109, D06305, doi:10.1029/2003JD004133, 2004. 24173

Grannas, A. M., Jones, A. E., Dibb, J., Ammann, M., Anastasio, C., Beine, H. J., Bergin, M., Bottenheim, J., Boxe, C. S., Carver, G., Chen, G., Crawford, J. H., Dominé, F., Frey, M. M., Guzmán, M. I., Heard, D. E., Helmig, D., Hoffmann, M. R., Honrath, R. E., Huey, L. G., Hutterli, M., Jacobi, H. W., Klán, P., Lefer, B., McConnell, J., Plane, J., Sander, R., Savarino, J., Shepson, P. B., Simpson, W. R., Sodeau, J. R., von Glasow, R., Weller, R., Wolff, E. W., and Zhu, T.: An overview of snow photochemistry: evidence, mechanisms and impacts, Atmos. Chem. Phys., 7, 4329–4373, doi:10.5194/acp-7-4329-2007, 2007. 24182

Hanson, D. R., Ravishankara, A. R., and Solomon, S.: Heterogeneous reactions in sulfuric acid aerosols: A framework for model calculations, J. Geophys. Res., 99, 3615–3629, 1994. 24178

Hausmann, M. and Platt, U.: Spectroscopic measurement of bromine oxide and ozone in the high Arctic during Polar Sunrise Experiment 1992, J. Geophys. Res., 99, 25399–25414, 1994. 24173

Helmig, D., Boylan, P., Johnson, B., Oltmans, S., Fairall, C., Staebler, R., Weinheimer, A., Orlando, J., Knapp, D. J., Montzka, D. D., Flocke, F., Frieß, U., Sihler, H., and Shepson, P. B.: Ozone dynamics and snow-atmosphere exchanges during ozone depletion events at Barrow, Alaska, J. Geophys. Res., 117, D20303, doi:10.1029/2012JD017531, 2012. 24173

Helmig, D., Oltmans, S., Carlson, D., Lamarque, J.-F., Jones, A. E., Labuschagne, C., Anlauf, K., and Hayden, K.: A review of surface ozone in the polar regions, Atmos. Environ., 41, 5138–5161, doi:10.1016/j.atmosenv.2006.09.053, 2007. 24173

Hönninger, G. and Platt, U.: Observations of BrO and its vertical distribution during surface ozone depletion at Alert, Atmos. Environ., 36, 2481–2489, 2002. 24173

Huff, A. K. and Abbatt, J. P. D.: Gas-phase Br_2 production in heterogeneous reactions of Cl_2, HOCl, and BrCl with halide-ice surfaces, J. Phys. Chem. A, 104, 7284–7293, 2000. 24174, 24180

Huff, A. K. and Abbatt, J. P. D.: Kinetics and product yields in the heterogeneous reactions of HOBr with ice surfaces containing NaBr and NaCl, J. Phys. Chem. A, 106, 5279–5287,2002. 24174, 24180

Impey, G., Mihele, C., Anlauf, K., Barrie, L., Hastie, D., and Shepson, P.: Measurements of photolyzable halogen compounds and bromine radicals during Polar Sunrise Experiment 1997, J. Atmos. Chem., 34, 21–37, 1999. 24187

Jacobi, H.-W., Frey, M. M., Hutterli, M. A., Bales, R. C., Schrems, O., Cullen, N. J., Steffen, K., and Koehler, C.: Measurements of hydrogen peroxide and formaldehyde exchange between the atmosphere and surface snow at Summit, Greenland, Atmos. Environ., 36, 2619–2628, doi:10.1016/S1352-2310(02)00106-1, 2002. 24182

Jobson, B. T., Niki, H., Yokouchi, Y., Bottenheim, J., Hopper, F., and Leaitch R.: Measurements of C_2-C_6 hydrocarbons during the Polar Sunrise 1992 Experiment: Evidence for Cl atom and Br atom chemistry, J. Geophys. Res., 99, 25355–25368, 1994. 24192

Jones, A. E., Weller, R., Wolff, E. W., and Jacobi, H.-W.: Speciation and rate of photochemical NO and NO_2 production in Antarctic snow, Geophys. Res. Lett., 27, 345–348, 2000. 24182

Jones, A. E., Weller, R., Anderson, P. S., Jacobi, H.-W., Wolff, E. W., Schrems, O., and Miller, H.: Measurements of NO_x emissions from the Antarctic snowpack, Geophys. Res. Lett., 28, 1499–1502, 2001. 24182

Jones, A. E., Anderson, P. S., Wolff, E. W., Turner, J., Rankin, A. M., and Colwell, S. R.: A role for newly forming sea ice in springtime polar tropospheric ozone loss? Observational evidence from Halley station, Antarctica, J. Geophys. Res., 111, D08306, doi:10.1029/2005JD006566, 2006. 24186

König, G.: Roughness length of an Antarctic ice shelf, Polarforschung, 55, 27–32, 1985.

Kreher, K., Johnston, P. V., Wood, S. W., Nardi, B., and Platt, U.: Ground-based measurements of tropospheric and stratospheric BrO at Arrival Heights, Antarctica, Geophys. Res. Lett., 24, 3021–3024, 1997. 24173

Langendörfer, U., Lehrer, E., Wagenbach, D., and Platt, U.: Observation of filterable bromine variabilities during Arctic tropospheric ozone depletion events in high time resolution, J. Atmos. Chem., 34, 39–54, 1999. 24183

Lehrer, E., Hönninger, G., and Platt, U.: A one dimensional model study of the mechanism of halogen liberation and vertical transport in the polar troposphere, Atmos. Chem. Phys., 4, 2427–2440, doi:10.5194/acp-4-2427-2004, 2004. 24180, 24183

Liao, J., Huey, L. G., Tanner, D. J., Brough, N., Brooks, S., Dibb, J. E., Stutz, J., Thomas, J. L., Lefer, B., Haman, C., and Gorham, K.: Observations of hydroxyl and peroxy radicals and the impact of BrO at Summit, Greenland in 2007 and 2008, Atmos. Chem. Phys., 11, 8577–8591, doi:10.5194/acp-11-8577-2011, 2011. 24173

Michalowski, B. A., Francisco, J. S., Li, S. M., Barrie, L. A., Bottenheim, J. W., and Shepson, P. B.: A computer model study of multiphase chemistry in the Arctic boundary layer during polar sunrise, J. Geophys. Res., 105, 15131–15145, 2000. 24173, 24181, 24192

Morin, S., Marion, G. M., von Glasow, R., Voisin, D., Bouchez, J., and Savarino, J.: Precipitation of salts in freezing seawater and ozone depletion events: a status report, Atmos. Chem. Phys., 8, 7317–7324, doi:10.5194/acp-8-7317-2008, 2008. 24173

Oltmans, S. J.: Surface ozone measurements in clean air, J. Geophys. Res., 86, 1174–1180, 1981. 24173

Oltmans, S. J., Schnell, R. C., Sheridan, P. J., Peterson, R. E., Li, S. M., Winchester, J. W., Tans, P. P., Sturges, W. T., Kahl, J. D., and Barrie, L. A.: Seasonal surface ozone and filterable bromine relationship in the high Arctic, Atmos. Environ., 23, 2431–2441, 1989. 24173

Oltmans, S. J., Johnson, B. J., and Harris, J. M.: Springtime boundary layer ozone depletion at Barrow, Alaska: Meteorological influence, year-to-year variation, and long-term change, J. Geophys. Res., 117, D00R18, doi:10.1029/2011JD016889, 2012. 24180

Perner, D., Arnold, T., Crowley, J., Klüpfel, T., Martinez, M., and Seuwen, R.: The measurements of active chlorine in the atmosphere by chemical amplification, J. Atmos. Chem., 34, 9–20, 1999. 24191

Piot, M. and von Glasow, R.: The potential importance of frost flowers, recycling on snow, and open leads for ozone depletion events, Atmos. Chem. Phys., 8, 2437–2467, doi:10.5194/acp-8-2437-2008, 2008. 24174

Piot, M. and von Glasow, R.: Modelling the multiphase near-surface chemistry related to ozone depletions in polar spring, J. Atmos. Chem., 64, 77–105, 2009. 24174

Platt, U. and Janssen, C.: Observation and role of the free radicals NO_3, ClO, BrO, and IO in the troposphere, Faraday Discuss., 100, 175–198, 1995. 24173

Platt, U. and Lehrer, E.: Arctic Tropospheric Ozone Chemistry, ARCTOC, Final Report of the EU-Project EV5V-CT93-0318, Heidelberg, 1997. 24173

Platt, U. and Moortgat, G. K.: Heterogeneous and homogeneous chemistry of reactive halogen compounds in the lower troposphere, J. Atmos. Chem., 34, 1–8, 1999. 24173

Platt, U. and Hönninger, G.: The role of halogen species in the troposphere, Chemosphere, 52, 325–338, 2003. 24173

Ramacher, B., Rudolph, J., and Koppmann, R.: Hydrocarbon measurements during tropospheric ozone depletion events: Evidence for halogen atom chemistry, J. Geophys. Res., 104, 3633–3653, 1999. 24192

Rankin, A. M., Wolff, E. W., and Martin, S.: Frost flowers: Implications for tropospheric chemistry and ice core interpretation, J. Geophys. Res., 107, 4683, doi:10.1029/2002JD002492, 2002. 24180

Röth, E. P.: A fast algorithm to calculate the photon flux in optically dense media for use in photochemical models, Ber. Bunsenges Phys. Chem., 96, 417–420, 1992. 24182

Röth, E. P.: Description of the anisotropic radiation transfer model ART to determine photodissociation coefficients, report, Inst. für Stratospharische Chem., Forsch. Julich, Julich, Germany, 2002. 24182

Sander, R. and Crutzen, P. J.: Model study indicating halogen activation and ozone destruction in polluted air masses transported to the sea, J. Geophys. Res., 101, 9121–9138, 1996. 24173, 24174, 24177, 24180

Sander, R., Vogt, R., Harris, G. W., and Crutzen, P. J.: Modelling the chemistry of ozone, halogen compounds, and hydrocarbons in the arctic troposphere during spring, Tellus B, 49, 522–532,1997. 24173

Sander, R., Rudich, Y., von Glasow, R., and Crutzen, P. J.: The role of $BrNO_3$ in marine tropospheric chemistry: A model study, Geophys. Res. Lett., 26, 2857–2860, 1999. 24189

Sander, R., Burrows, J., and Kaleschke, L.: Carbonate precipitation in brine – a potential trigger for tropospheric ozone depletion events, Atmos. Chem. Phys., 6, 4653–4658, doi:10.5194/acp-6-4653-2006, 2006. 24173

Schwartz, S. E.: Mass-transport considerations pertinent to aqueous-phase reactions of gases in liquid-water clouds, in: Chemistry of Multiphase Atmospheric Systems, W. Jaeschke, Ed., Springer, Heidelberg, 415–471, 1986. 24177

Seinfeld, J. H. and Pandis S. N.: Atmospheric chemistry and physics: from air pollution to climate change, John Wiley and Sons, New York, 1988. 24179

Simpson, W. R., von Glasow, R., Riedel, K., Anderson, P., Ariya, P., Bottenheim, J., Burrows, J., Carpenter, L. J., Frieß, U., Goodsite, M. E., Heard, D., Hutterli, M., Jacobi, H.-W., Kaleschke, L., Neff, B., Plane, J., Platt, U., Richter, A., Roscoe, H., Sander, R., Shepson, P., Sodeau, J., Steffen, A., Wagner, T., and Wolff, E.: Halogens and their role in polar boundary-layer ozone depletion, Atmos. Chem. Phys., 7, 4375–4418, doi:10.5194/acp-7-4375-2007, 2007. 24173, 24186

Solberg, S., Schmidtbauer, N., Semb, A., Stordal, F., and Hov, Ø.: Boundary-layer ozone depletion as seen in the Norwegian Arctic in spring, J. Atmos. Chem., 23, 301–332, 1996. 24192

Spicer, C. W., Plastridge, R. A., Foster, K. L., Finlayson-Pitts, B. J., Bottenheim, J. W., Grannas, A. M., and Shepson, P. B.: Molecular halogens before and during ozone depletion events in the Arctic at polar sunrise: concentration and sources, Atmos. Environ., 36, 2721–2731, 2002. 24192

Staebler, R., Toom-Sauntry, D., Barrie, L., Langendörfer, U., Lehrer, E., Li, S.-M., and Clark, H. D.: Physical and chemical characteristics of aerosols at Spitsbergen in the spring of 1996, J. Geophys. Res., 104, 5515–5529, 1999. 24178

Stull, R. B.: An introduction to boundary layer meteorology, Kluwer Academic Publishers, Dordrecht, The Netherlands, 666 pp., 1988. 24180, 24183

Tang, T. and McConnell, J. C., Autocatalytic release of bromine from Arctic snow pack during polar sunrise, Geophys. Res. Lett., 23, 2633–2636, 1996. 24173

Thomas, J. L., Stutz, J., Lefer, B., Huey, L. G., Toyota, K., Dibb, J. E., and von Glasow, R.: Modeling chemistry in and above snow at Summit, Greenland – Part 1: Model description and results, Atmos. Chem. Phys., 11, 4899–4914, doi:10.5194/acp-11-4899-2011, 2011. 24174

Toyota, K., McConnell, J. C., Lupu, A., Neary, L., McLinden, C. A., Richter, A., Kwok, R., Semeniuk, K., Kaminski, J. W., Gong, S.-L., Jarosz, J., Chipperfield, M. P., and Sioris, C. E.: Analysis of reactive bromine production and ozone depletion in the Arctic boundary layer using 3-D simulations with GEM-AQ: inference from synoptic-scale patterns, Atmos. Chem. Phys., 11, 3949–3979, doi:10.5194/acp-11-3949-2011, 2011. 24174

Toyota, K., McConnell, J. C., Staebler, R. M., and Dastoor, A. P.: Air-snowpack exchange of bromine, ozone and mercury in the springtime Arctic simulated by the 1-D model PHANTAS – Part 1: In-snow bromine activation and its impact on ozone, Atmos. Chem. Phys. Discuss., 13, 20341–20418, doi:10.5194/acpd-13-20341-2013, 2013. 24174

Tuckermann, M., Ackermann, R., Gölz, C., Lorenzen-Schmidt, H., Senne, T., Stutz, J., Trost, B., Unold, W., and Platt, U.: DOAS-observation of halogen radical-catalyzed arctic boundary layer ozone destruction during the ARCTOC-campaigns 1995 and 1996 in Ny-Ålesund, Spitsbergen, Tellus, 49B, 533–555, 1997. 24173, 24186

Turanyi, T.: KINAL: A program package for kinetic analysis of reaction mechanisms, Computers and Chemistry, 14, 253–254, 1990. 24175

Valko, P. and Vajda, S.: An extended ODE solver for sensitivity calculations, Computers and Chemistry, 8, 255–271, 1984. 24176

Wagner, T., Ibrahim, O., Sinreich, R., Frieß, U., von Glasow, R., and Platt, U.: Enhanced tropospheric BrO over Antarctic sea ice in mid winter observed by MAX-DOAS on board the research vessel Polarstern, Atmos. Chem. Phys., 7, 3129–3142, doi:10.5194/acp-7-3129-2007, 2007. 24173

Wayne, R. P., Poulet, G., Biggs, P., Burrows, J. P., Cox, R. A., Crutzen, P. J., Hayman, G. D., Jenkin, M. E., Le Bras, G., Moortgat, G. K., Platt, U., and Schindler, R. N.: Halogen oxides:

Radicals, sources and reservoirs in the laboratory and in the atmosphere, Atmos. Environ., 29, 2677–2884, 1995. 24173

Wennberg, P. O.: Atmospheric chemistry: Bromine explosion, Nature, 397, 299–301, 1999. 24173

Yang, X., Cox, R. A., Warwick, N. J., Pyle, J. A., Carver, G. D., O'Connor, F. M., and Savage., N. H.: Tropospheric bromine chemistry and its impacts on ozone: a model study, J. Geophys. Res., 110, D23311, doi:10.1029/2005JD006244, 2005. 24180

Yang, X., Pyle, J. A., and Cox, R. A.: Sea salt aerosol production and bromine release: Role of snow on sea ice, Geophys. Res. Lett., 35, L16815, doi:10.1029/2008GL034536, 2008. 24174

Yang, X., Pyle, J. A., Cox, R. A., Theys, N., and Van Roozendael, M.: Snow-sourced bromine and its implications for polar tropospheric ozone, Atmos. Chem. Phys., 10, 7763–7773, doi:10.5194/acp-10-7763-2010, 2010. 24174

Zeng, T., Wang, Y., Chance, K., Browell, E. V., Ridley, B. A., and Atlas, E. L.: Widespread persistent near-surface ozone depletion at northern high latitudes in spring, Geophys. Res. Lett., 30, 2298, doi:10.1029/2003GL018587, 2003. 24174

Zhao, T. L., Gong, S. L., Bottenheim, J. W., McConnell, J. C., Sander, R., Kaleschke, L., Richter, A., Kerkweg, A., Toyota, K., and Barrie, L. A.: A three-dimensional model study on the production of BrO and Arctic boundary layer ozone depletion, J. Geophys. Res., 113, D24304, doi:10.1029/2008JD010631, 2008. 24174

Table 1. Emission fluxes from the snow.

Species	Emission rates [molec. $cm^{-2}s^{-1}$]
NO	1.6×10^7
NO_2	1.6×10^7
HONO	1.6×10^7
H_2O_2	1.6×10^8
HCHO	6.0×10^7

Table 2. Initial gas composition.

Species	Mixing ratio
O_3	40 ppb
Br_2	0.3 ppt
HBr	0.01 ppt
CH_4	1.9 ppm
CO_2	371 ppm
CO	132 ppb
HCHO	100 ppt
CH_3CHO	100 ppt
C_2H_6	2.5 ppb
C_2H_4	100 ppt
C_2H_2	600 ppt
C_3H_8	1.2 ppb
NO	5 ppt
NO_2	10 ppt
Cl_2	0.3 ppt
HCl	0.01 ppt

Title Page
Abstract | Introduction
Conclusions | References
Tables | Figures
◀| |▶
◀ ▶
Back | Close
Full Screen / Esc
Printer-friendly Version
Interactive Discussion

Table 3. List of ozone relevant reactions (Type F: Ozone formation; Type D: Ozone depletion).

Reaction	No.	Type
$O_3 + h\nu \rightarrow O + O_2$	(R1)	D
$O + O_2 \rightarrow O_3$	(R3)	F
$Br + O_3 \rightarrow BrO + O_2$	(R5)	D
$BrO + h\nu \rightarrow Br + O_3$	(R7)	F
$OH + O_3 \rightarrow HO_2 + O_2$	(R27)	D
$OH + OH + O_2 \rightarrow H_2O + O_3$	(R30)	F
$HO_2 + O_3 \rightarrow OH + 2O_2$	(R31)	D
$C_2H_4 + O_3 \rightarrow HCHO + CO + H_2O$	(R36)	D
$2OH + O_2 \xrightarrow{M} H_2O + O_3$	(R54)	F

Table 4. List of important NO_x relevant reactions (Type F: NO_x formation; Type D: NO_x depletion).

Reaction	No.	Type
$HO_2 + NO_2 \rightarrow HNO_4$	(R62)	D
$HNO_4 \rightarrow HO_2 + NO_2$	(R63)	F
$Br + NO_2 \rightarrow BrNO_2$	(R77)	D
$BrO + NO_2 \rightarrow BrONO_2$	(R79)	D
$BrONO_2 + h\nu \rightarrow BrO + NO_2$	(R81)	F
$BrNO_2 + h\nu \rightarrow Br + NO_2$	(R82)	F
$HNO_3 + h\nu \xrightarrow{\text{aerosol}} NO_2 + OH$	(R85)	F

Table 5. Overview of NO_x relevant reaction cycles.

Reaction	No.	Cycle (Period)
$HO_2 + NO_2 \rightarrow HNO_4$ $HNO_4 \rightarrow HO_2 + NO_2$	(R62) (R63)	N-I (Induction)
$BrO + NO_2 \rightarrow BrONO_2$ $BrONO_2 + h\nu \rightarrow BrO + NO_2$ $BrONO_2 \xrightarrow{H_2O} HOBr + HNO_3$ $HNO_3 \xrightarrow{\text{aerosol}} NO_2 + OH$	(R79) (R81) (R83, R86) (R85)	N-II (Depletion)
$Br + NO_2 \rightarrow BrNO_2$ $BrNO_2 + h\nu \rightarrow Br + NO_2$	(R77) (R82)	N-III (After Depletion)

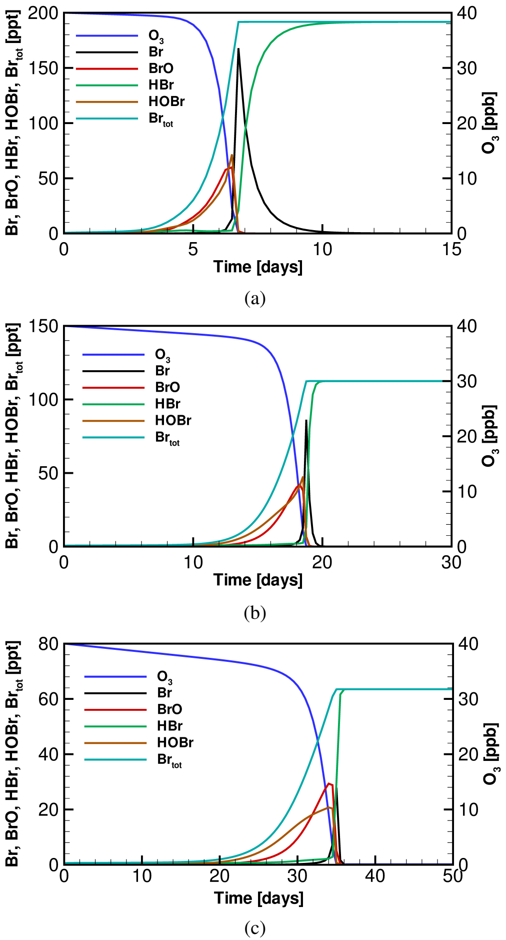

Fig. 1. Time variation of mixing ratio of ozone and bromine using the bromine mechanism for the boundary layer height of **(a)** 200 m **(b)** 500 m **(c)** 1000 m.

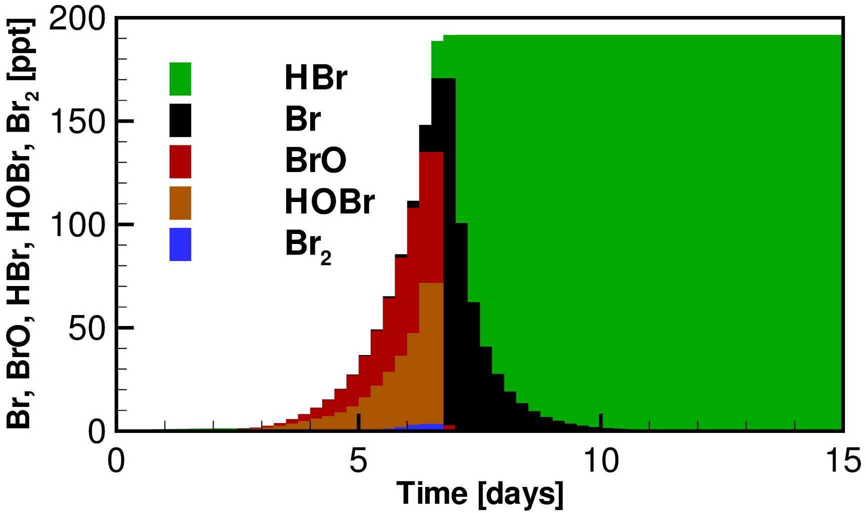

Fig. 2. Mixing ratio of ozone and bromine using the bromine mechanism for the boundary layer height of 200 m.

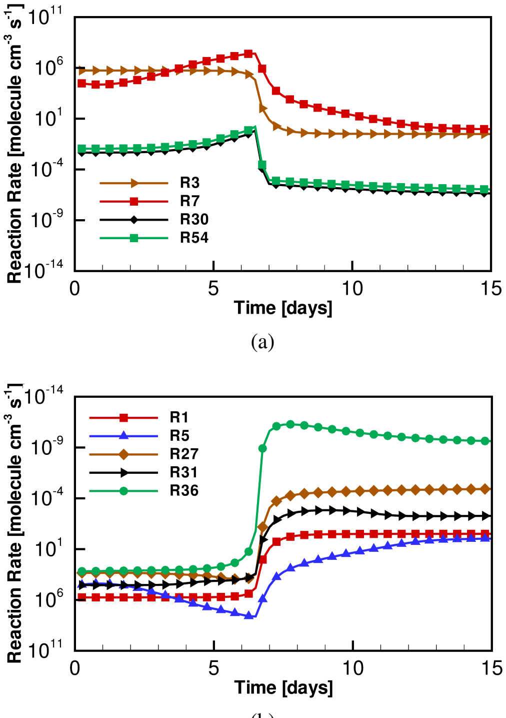

(a)

(b)

Fig. 3. Temporal behavior of ozone relevant reaction rates in a 200 m boundary layer height: **(a)** formation **(b)** depletion. Note that a reverse direction of vertical axis is used in the bottom panel.

(R5) $Br + O_3 \rightarrow BrO + O_2$
(R6) $Br_2 + h\nu \rightarrow 2Br$
(R7) $BrO + h\nu \rightarrow Br + O_3$
(R8) $BrO + BrO \rightarrow 2Br + O_2$
(R9) $BrO + BrO \rightarrow Br_2 + O_2$
(R10) $BrO + HO_2 \rightarrow HOBr + O_2$
(R11) $HOBr + h\nu \rightarrow Br + OH$
(R12) $CO + OH + O_2 \rightarrow HO_2 + CO_2$
(R13) $Br + HO_2 \rightarrow HBr + O_2$
(R14) $HOBr + HBr \xrightarrow{\text{aerosol}} Br_2 + H_2O$
(R15) $HOBr + H^+ + Br^- \xrightarrow{\text{ice/snow}} Br_2 + H_2O$
(R16) $Br + HCHO + O_2 \rightarrow HBr + CO + HO_2$
(R17) $Br + CH_3CHO + O_2 \rightarrow HBr + CH_3CO_3$
(R18) $Br + OH \rightarrow HOBr + Br$
(R19) $HBr + OH \rightarrow H_2O + Br$
(R20) $Br + C_2H_2 + 3O_2 \rightarrow 2CO + 2HO_2 + Br$
(R21) $Br + C_2H_2 + 2O_2 \rightarrow 2CO + 2HO_2 + HBr$
(R22) $Br + C_2H_4 + 3.5O_2 \rightarrow 2CO + 2HO_2 + Br + H_2O$
(R23) $Br + C_2H_4 + 2.5O_2 \rightarrow 2CO + HO_2 + HBr + H_2O$
(R24) $CH_4 + OH + O_2 \rightarrow CH_3O_2 + H_2O$
(R25) $BrO + CH_3O_2 \rightarrow Br + HCHO + HO_2$
(R26) $BrO + CH_3O_2 \rightarrow HOBr + HCHO + 0.5O_2$

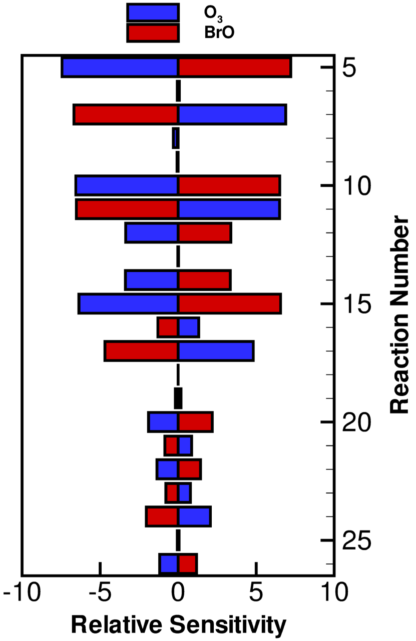

Fig. 4. Relative sensitivities of ozone and BrO concentrations for bromine containing reactions at day 6 for a 200 m boundary layer height.

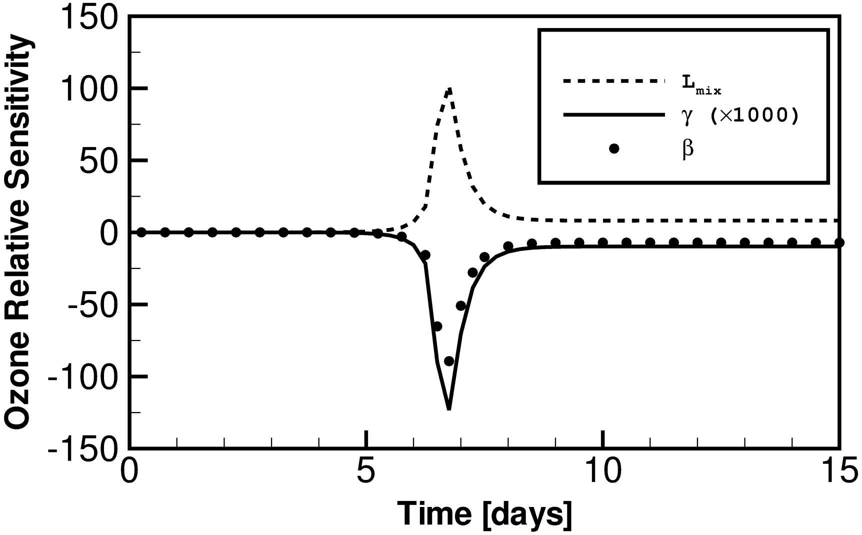

Fig. 5. Temporal evolution of ozone concentration sensitivities for mixing heigh L_{mix}, uptake coefficient γ, and reactive surface ratio β.

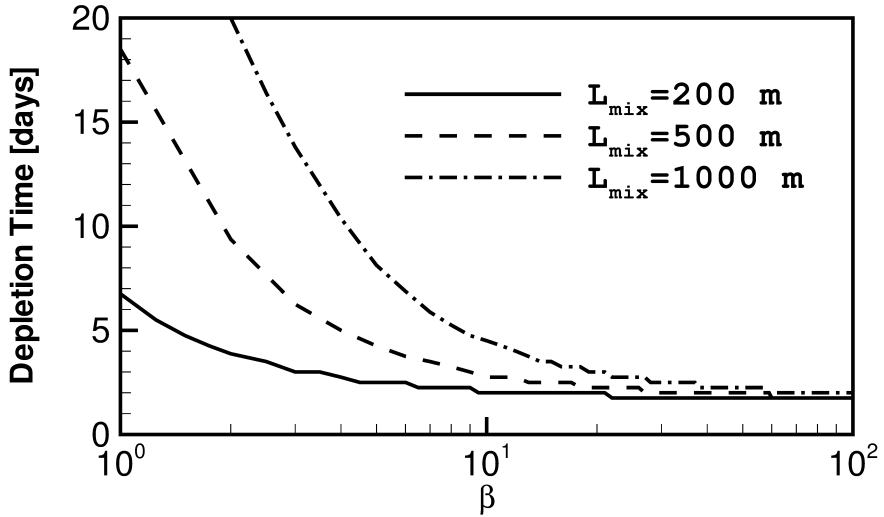

Fig. 6. Impact of the reactive surface ratio on the ozone depletion rate.

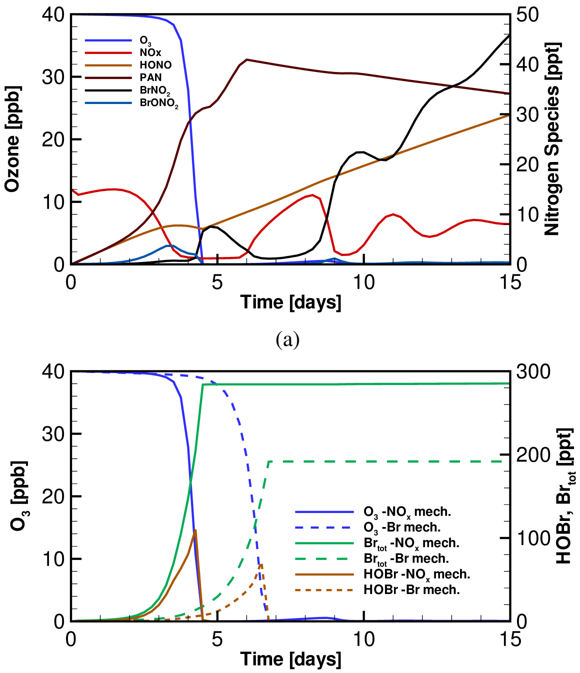

(a)

(b)

Fig. 7. Time variation of ozone, nitrogen containing species and bromine concentrations for a boundary layer height of 200 m.

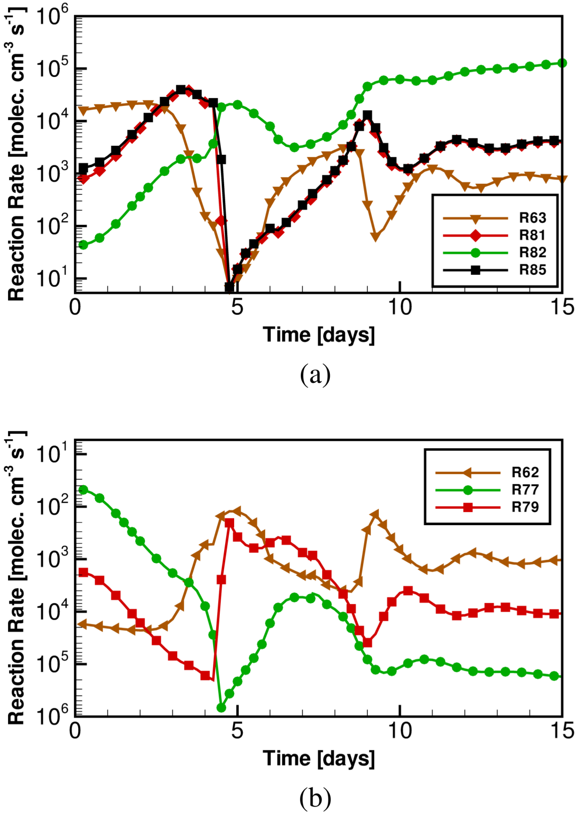

Fig. 8. Temporal change of NO_x relevant reaction rates in 200 m boundary layer height: **(a)** formation **(b)** depletion.

ACPD
13, 24171–24222, 2013

(R56)	$NO + O_3 \rightarrow NO_2 + O_2$
(R57)	$NO + HO_2 \rightarrow NO_2 + OH$
(R58)	$NO_2 + O_3 \rightarrow NO_3 + O_2$
(R59)	$NO_2 + OH \rightarrow HNO_3$
(R60)	$NO + NO_3 \rightarrow 2NO_2$
(R61)	$HONO + OH \rightarrow NO_2 + H_2O$
(R62)	$HO_2 + NO_2 \rightarrow HNO_4$
(R63)	$HNO_4 \rightarrow NO_2 + HO_2$
(R64)	$HNO_4 + OH \rightarrow NO_2 + H_2O + O_2$
(R65)	$NO + OH \rightarrow HONO$
(R66)	$OH + NO_3 \rightarrow NO_2 + HO_2$
(R67)	$HNO_3 + h\nu \rightarrow NO_2 + OH$
(R68)	$NO_2 + O_2 + h\nu \rightarrow NO + O_3$
(R69)	$NO_3 + h\nu \rightarrow NO_2 + O$
(R70)	$NO_3 + h\nu \rightarrow NO + O_2$
(R71)	$NO + CH_3O_2 + O_2 \rightarrow HCHO + HO_2 + NO_2$
(R72)	$NO_3 + CH_3OH + O_2 \rightarrow HCHO + HO_2 + HNO_3$
(R73)	$NO_3 + HCHO + O_2 \rightarrow CO + HO_2 + HNO_3$
(R74)	$NO + C_2H_5O_2 + O_2 \rightarrow CH_3CHO + NO_2 + HO_2$
(R75)	$NO + CH_3CO_3 + O_2 \rightarrow CH_3O_2 + NO_2 + CO_2$
(R76)	$NO_2 + CH_3CO_3 \rightarrow PAN$
(R77)	$Br + NO_2 \rightarrow BrNO_2$
(R78)	$Br + NO_3 \rightarrow BrO + NO_2$
(R79)	$BrO + NO_2 \rightarrow BrONO_2$
(R80)	$BrO + NO \rightarrow Br + NO_2$
(R81)	$BrONO_2 + h\nu \rightarrow NO_3 + Br$
(R82)	$BrNO_2 + h\nu \rightarrow NO_2 + Br$
(R83)	$BrONO_2 + H_2O \xrightarrow{\text{aerosol}} HOBr + HNO_3$
(R84)	$PAN + h\nu \rightarrow NO_2 + CH_3CO_3$
(R85)	$HNO_3 + h\nu \xrightarrow{\text{aerosol}} OH + NO_2$
(R86)	$BrONO_2 + H_2O \xrightarrow{\text{ice/snow}} HOBr + HNO_3$

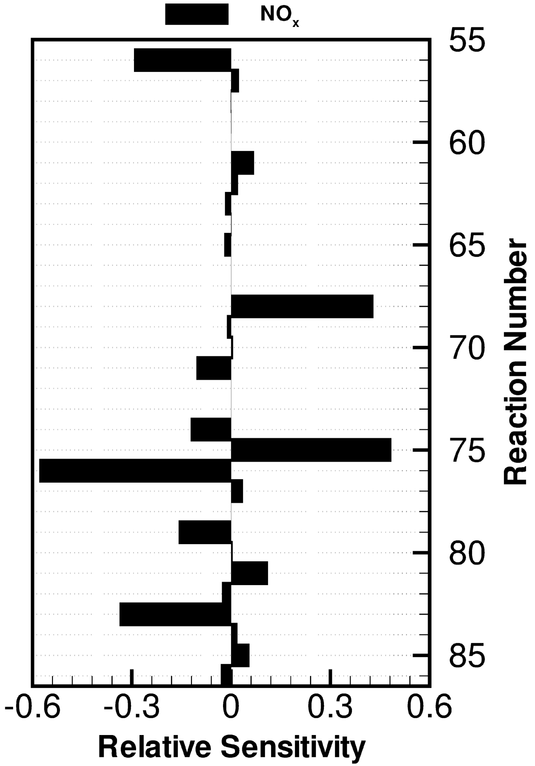

Fig. 9. Relative sensitivities of NO_x concentrations at day 4 for a boundary layer height of 200 m.

(R56) $NO + O_3 \rightarrow NO_2 + O_2$
(R57) $NO + HO_2 \rightarrow NO_2 + OH$
(R58) $NO_2 + O_3 \rightarrow NO_3 + O_2$
(R59) $NO_2 + OH \rightarrow HNO_3$
(R60) $NO + NO_3 \rightarrow 2NO_2$
(R61) $HONO + OH \rightarrow NO_2 + H_2O$
(R62) $HO_2 + NO_2 \rightarrow HNO_4$
(R63) $HNO_4 \rightarrow NO_2 + HO_2$
(R64) $HNO_4 + OH \rightarrow NO_2 + H_2O + O_2$
(R65) $NO + OH \rightarrow HONO$
(R66) $OH + NO_3 \rightarrow NO_2 + HO_2$
(R67) $HNO_3 + h\nu \rightarrow NO_2 + OH$
(R68) $NO_2 + O_2 + h\nu \rightarrow NO + O_3$
(R69) $NO_3 + h\nu \rightarrow NO_2 + O$
(R70) $NO_3 + h\nu \rightarrow NO + O_2$
(R71) $NO + CH_3O_2 + O_2 \rightarrow HCHO + HO_2 + NO_2$
(R72) $NO_3 + CH_3OH + O_2 \rightarrow HCHO + HO_2 + HNO_3$
(R73) $NO_3 + HCHO + O_2 \rightarrow CO + HO_2 + HNO_3$
(R74) $NO + C_2H_5O_2 + O_2 \rightarrow CH_3CHO + NO_2 + HO_2$
(R75) $NO + CH_3CO_3 + O_2 \rightarrow CH_3O_2 + NO_2 + CO_2$
(R76) $NO_2 + CH_3CO_3 \rightarrow PAN$
(R77) $Br + NO_2 \rightarrow BrNO_2$
(R78) $Br + NO_3 \rightarrow BrO + NO_2$
(R79) $BrO + NO_2 \rightarrow BrONO_2$
(R80) $BrO + NO \rightarrow Br + NO_2$
(R81) $BrONO_2 + h\nu \rightarrow NO_3 + Br$
(R82) $BrNO_2 + h\nu \rightarrow NO_2 + Br$
(R83) $BrONO_2 + H_2O \overset{\text{aerosol}}{\longrightarrow} HOBr + HNO_3$
(R84) $PAN + h\nu \rightarrow NO_2 + CH_3CO_3$
(R85) $HNO_3 + h\nu \overset{\text{aerosol}}{\longrightarrow} OH + NO_2$
(R86) $BrONO_2 + H_2O \overset{\text{ice/snow}}{\longrightarrow} HOBr + HNO_3$

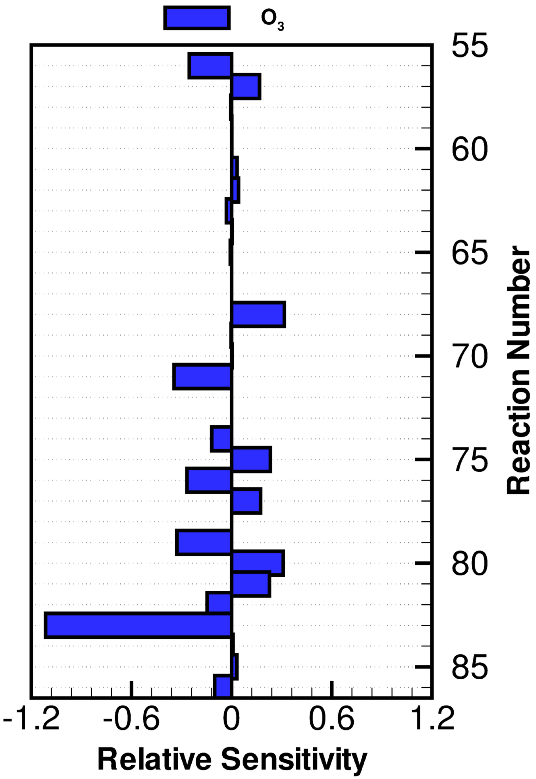

Fig. 10. Relative sensitivities of O_3 concentrations at day 4 for a boundary layer height of 200 m.

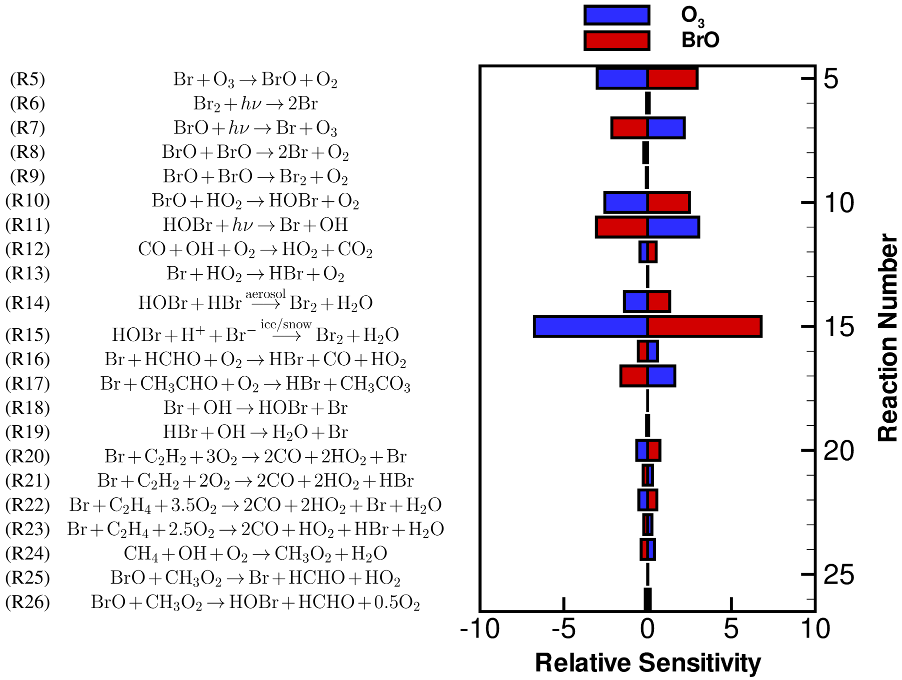

Fig. 11. Relative sensitivities of O_3 and BrO concentrations at day 4 for a boundary layer height of 200 m.

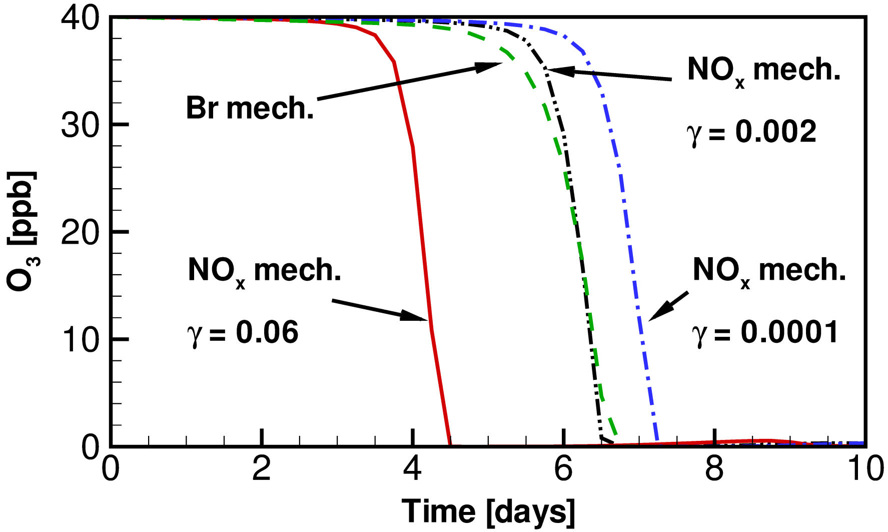

Fig. 12. Ozone depletion rates with different values of $BrONO_2$ hydrolysis uptake coefficient.

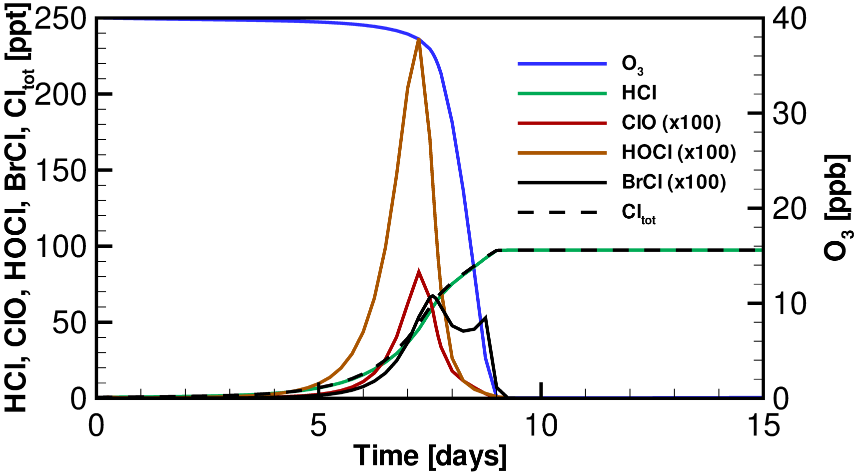

Fig. 13. Time evolution of ozone, chlorine containing species and total chlorine concentration for a boundary layer height of 200 m.

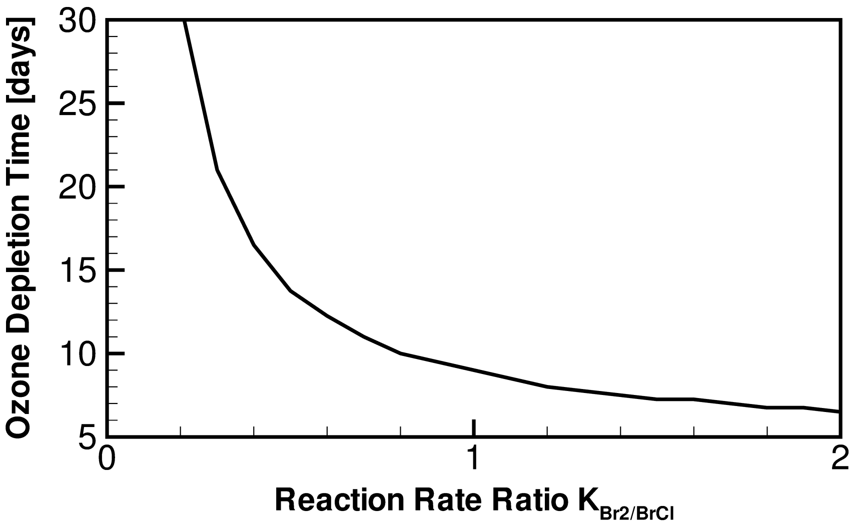

Fig. 14. Impact of the reaction rate ratio of (R15) and (R129), $K_{Br_2/BrCl}$, on the ozone depletion time.

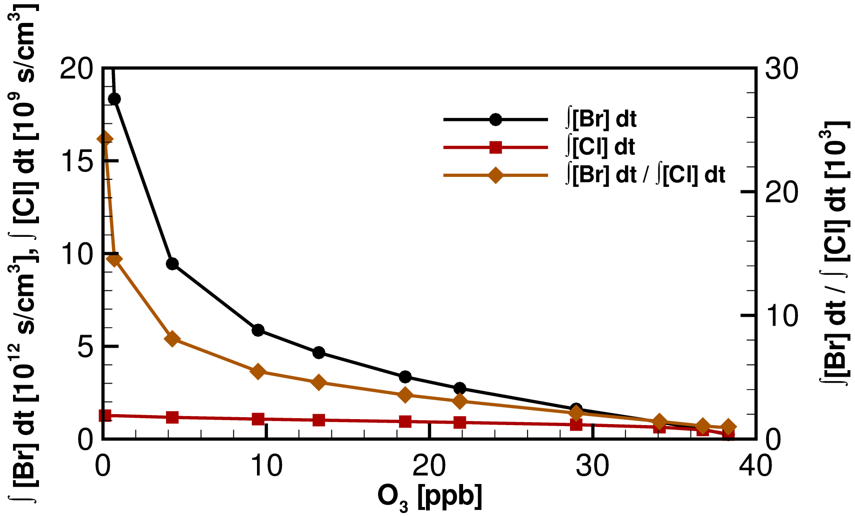

Fig. 15. Time integrated halogen atom concentration and the [Br] / [Cl] ratio versus the ozone mixing ratio.